

Twisted-light-ion interaction: the role of longitudinal fields

Guillermo F. Quinteiro,¹ Ferdinand Schmidt-Kaler,² and Christian T. Schmiegelow¹

¹*Departamento de Física and IFIBA, FCEN, Universidad de Buenos Aires, Ciudad Universitaria, Pabellón I, 1428 Ciudad de Buenos Aires, Argentina**

²*Institut für Physik, Universität Mainz, Staudingerweg 7, 55128 Mainz, Germany*

The propagation of light beams is well described using the paraxial approximation, where field components along the propagation direction are usually neglected. For strongly inhomogeneous or shaped light fields, however, this approximation may fail, leading to intriguing variations of the light-matter interaction. This is the case of twisted light having opposite orbital and spin angular momenta. We compare experimental data for the excitation of a quadrupole transition in a single trapped $^{40}\text{Ca}^+$ ion by Schmiegelow et al, Nat. Comm. 7, 12998 (2016), with a complete model where longitudinal components of the electric field are taken into account. Our model matches the experimental data and excludes by 11 standard deviations the approximation of complete transverse field. This demonstrates the importance of all field components in the interaction of twisted light with matter.

The full vector character of the electromagnetic field is responsible for a variety of basic physical processes, such as those occurring in near-field optics and the propagation of focused beams close to the diffraction limit [1, 2]. Moreover, electromagnetic fields with components in all possible directions play a special role in applied science. For example, the sub-diffraction-limited focusing of radially polarized beams producing strong longitudinal fields [3] can be used to improve material processing [4, 5]. Also, longitudinal fields have seen application in Raman spectroscopy [6], optical tweezers [7], and have been used to observe circular dichroism in non-chiral nanostructures [8].

Light carrying orbital angular momentum, known also as twisted light (TL) or optical vortices, has introduced us to a new realm of structured light [9–13]. An unusual property of TL has to do with the relative orientation of the photon's angular momenta. When the orbital and spin angular momenta are antiparallel to each other, longitudinal field components become important. As a result, the light-matter interaction is different for parallel or anti-parallel momenta beams. This has been suggested in several theoretical articles dealing with tightly-focused TL [14, 15] and TL-related beams [16–20]. Longitudinal fields in structured beams promise new applications, such as the control of the spin state of electrons or impurities in quantum dots [14, 21], and the excitation of intersub-band [22] transitions in quantum wells [23].

For propagating fields that are not tightly focused the complexity of the full vector model can be reduced, still retaining an excellent description of the physics under consideration. In the paraxial approximation [24] one assumes that the transverse profile changes slowly along the propagation direction, here z . To lowest order in the ratio of wavelength to beam waist the electric and magnetic fields have no longitudinal component [25, 26]. Although very common, such a strong assumption is not always correct. Theory shows that Laguerre-Gaussian (LG) beams, the paradigmatic paraxial TL, has a non-

negligible longitudinal component when spin and orbital angular momenta are opposite to each other [25, 27]. In this article we show that the correct description of the light-matter interaction between a single ion and a paraxial LG beam requires the inclusion of the longitudinal electric-field component, when the beam is in the antiparallel momenta configuration. Thus, longitudinal field components do matter even in the paraxial approximation, and may lead to unexpected applications, for example to chiral quantum optics [28, 29].

Before engaging in the light-matter model and comparison with experiments, we briefly discuss Laguerre-Gaussian modes. These modes are solutions of the paraxial wave equation in cylindrical coordinates $\{r, \phi, z\}$, and are perhaps the most studied of all optical-vortex beams, for they can be easily produced from conventional laser beams using computer generated holograms, cylindrical lenses, Q-plates, etc. [30]. The starting point for the derivation of the electromagnetic field is a transverse Lorentz-gauge vector potential $\mathbf{A}(\mathbf{r}, t) = A_0 \epsilon u(\mathbf{r}) \exp(-i\omega t + ikz) + c.c.$, with polarization $\epsilon = \epsilon_x \hat{x} + \epsilon_y \hat{y}$ and mode $u(\mathbf{r})$ constructed from a combination of a generalized Laguerre polynomial, a Gaussian function, a polynomial and a phase factor [30, 31]. Using the Lorenz condition, a scalar potential can be deduced. From vector and scalar potentials, the electric and magnetic fields are calculated. In problems involving the interaction with small objects which are centered with respect to the beam axis, the full lateral spatial extend of the beam is irrelevant, and one can simplify the beam's profile without significant loss of precision. This is the case for the experiment here discussed [32]. The positive part of the electric field of a circularly polarized LG beam close to the phase singularity at $r = 0$ is thus

$$\mathbf{E}^{(+)}(\mathbf{r}) = \frac{E_0}{\sqrt{2}} \left\{ (\hat{x} + i\sigma\hat{y})u(\mathbf{r}) + \frac{i}{k} [\partial_x u(\mathbf{r}) + \partial_y u(\mathbf{r})] \hat{z} \right\} e^{ikz} \quad (1)$$

$$\text{with: } u(\mathbf{r}) = \frac{\sqrt{2}^{|l|+1}}{\sqrt{\pi} |\ell|! w_0^{|\ell|+1}} (x^2 + y^2)^{\frac{|\ell|}{2}} e^{i\ell \arctan(y/x)}.$$

Here $\mathbf{E}(\mathbf{r}, t) = \mathbf{E}^{(+)}(\mathbf{r})e^{-i\omega t} + \text{c.c.}$, σ is the spin index or handedness of circular polarization, w_0 is the waist, k is the wave number in the longitudinal direction, and the integer ℓ is the orbital angular momentum index. In cylindrical coordinates $\{r, \varphi, z\}$ the resulting field can be conveniently separated into transverse $\mathbf{E}_{\perp}^{(+)}(\mathbf{r})$ and longitudinal $E_z^{(+)}(\mathbf{r})$ components. One obtains

$$\mathbf{E}_{\perp}^{(+)}(\mathbf{r}) = (\hat{x} + i\sigma\hat{y}) \frac{E_0}{\sqrt{\pi} |\ell|! w_0} \left(\frac{\sqrt{2}}{w_0} r \right)^{|\ell|} \times e^{i\ell\varphi} e^{ikz} \quad (2a)$$

$$E_z^{(+)}(\mathbf{r}) = -i\hat{z} (\ell\sigma - |\ell|) (1 - \delta_{\ell,0}) \frac{E_0}{\sqrt{\pi} |\ell|! w_0} \frac{\sqrt{2}}{w_0 k} \times \left(\frac{\sqrt{2}}{w_0} r \right)^{|\ell|-1} e^{i(\ell+\sigma)\varphi} e^{ikz}, \quad (2b)$$

Here one can directly see that the longitudinal component is only present when spin and orbital angular momenta are counter rotating, i. e. for $(\ell\sigma - |\ell|) = -2|\ell|$. In this situation is in fact crucial to take into account the longitudinal field to accurately describe quantitatively the atom-photon interaction. Also clear is that $E_z^{(+)}(\mathbf{r})$ is of higher order in the paraxial parameter $1/(w_0 k)$.

Intriguing features of light fields can be sensed by matter, especially by atoms. Thus an accurate theory of light-matter interaction which considers the full vector properties of the beam is needed. In particular we consider the interaction of such light fields with a single atom which is well localized with respect to the beam size. We will consider ions or atoms cooled below they Lamb-Dicke limit so it is well justified to neglect linear momentum transfer to the atom's center of mass.

The light-matter interaction for beams with $|\ell| = 0, 1$ is dominated by the electric field. In the Poincaré gauge, the interaction Hamiltonian results from the scalar potential $U(\mathbf{r}, t) = -\int_0^1 \mathbf{r} \cdot \mathbf{E}(u\mathbf{r}, t) du$ [33], where the explicit expressions for the electric field Eqs. (2a)-(2b) are used. Transforming to spherical coordinates $\{\rho, \varphi, \theta\}$ and separating the interaction Hamiltonian $H_I = qU(\mathbf{r}, t)$ into in-plane and z sections result in the following. For $\ell = 0$:

$$H_{I\perp}^{(+)} = -\alpha\rho \sin(\theta) e^{i\sigma\varphi} \int_0^1 u e^{ikup \cos(\theta)} du \quad (3a)$$

$$H_{Iz}^{(+)} = 0, \quad (3b)$$

where $\alpha = \sqrt{2/\pi} q E_0 / w_0^2$, with $q = -|q_e|$ the electric

charge. For $\ell = \pm 1$:

$$H_{I\perp}^{(+)} = -\alpha\rho^2 \sin^2(\theta) e^{i(|\ell|/\ell+\sigma)\varphi} \int_0^1 u e^{ikup \cos(\theta)} du \quad (4a)$$

$$H_{Iz}^{(+)} = -i\delta_{\ell,-\sigma} \alpha\rho \cos(\theta) \frac{2}{k} \int_0^1 e^{ikup \cos(\theta)} du. \quad (4b)$$

The oscillating time dependence appears in $H_I = H_I^{(+)} e^{-i\omega t} + \text{c.c.}$. The positive part of H_I is sufficient to calculate transition matrix elements in the rotating wave approximation [34].

In the experiment a LG beam with wavelength near $\lambda = 729$ nm was focused to $w_0 = 2.7 \mu\text{m}$. This focus size is well above the optical diffraction limit. A single ion was laser-cooled to a wavepacket position uncertainty of $\Delta r = 60$ nm, positioned at the center of the vortex field and the quadrupole $S_{1/2}$ to $D_{5/2}$ transition was excited.

As is usual, due to the small size of the atom with respect to the wavelength of the exciting laser, a Taylor approximation of $\exp[ikup \cos(\theta)]$ is justified. However, the expansion has to be treated differently for the in-plane and z sections of the interaction. We will be concentrating on quadrupole transitions where the initial and final state have the same parity. This causes the transition matrix elements to vanish at lowest order in the coordinates. The matrix elements governing these transitions are thus those with quadratic dependence on the coordinates.

When $\ell = 0$ the transitions allowed by angular momentum selection rules are those with a change in projection of angular momentum in the z direction: $\Delta m = \pm 1$. In Fig. 1a these are labelled $\{b, d\}$ and $\{g, i\}$. These transitions are governed by Eq. 3a. The zero order term in the expansion of the exponential yields a Hamiltonian linear in the coordinates, and vanishes for the quadrupole transition. The transition is thus mediated by the following term in the expansion: $H_{I\perp}^{(+)} \simeq -i(\alpha k \rho^2 / 3) \sin(\theta) \cos(\theta) e^{i\sigma\varphi}$.

In the case $\ell = \pm 1$, in-plane and/or longitudinal interactions may induce the transitions with no change or a change of two units of angular momentum of the ion ($\Delta m = 0, \pm 2$) depending on the signs of the polarization (σ) and the sense of rotation of the LG beam (the sign of ℓ). These transitions are labelled $\{a, c, e\}$ and $\{f, h, j\}$ in Fig. 1a. Following the same reasoning as before, we must consider the first-order term $\exp[ikup \cos(\theta)] \simeq ikup \cos(\theta)$ for transitions induced by H_{Iz} , but it suffices to consider the zero-order term $\exp[ikup \cos(\theta)] \simeq 1$ for $H_{I\perp}$.

It is worth noting that even though different approximations to $\exp[ikup \cos(\theta)]$ were used, both interaction terms $H_{I\perp}^{(+)}$ and $H_{Iz}^{(+)}$ are of the same magnitude, a fact that will become evident when the numerical evaluations are performed. Moreover, the ratio of these two components does not depend on the focus size.

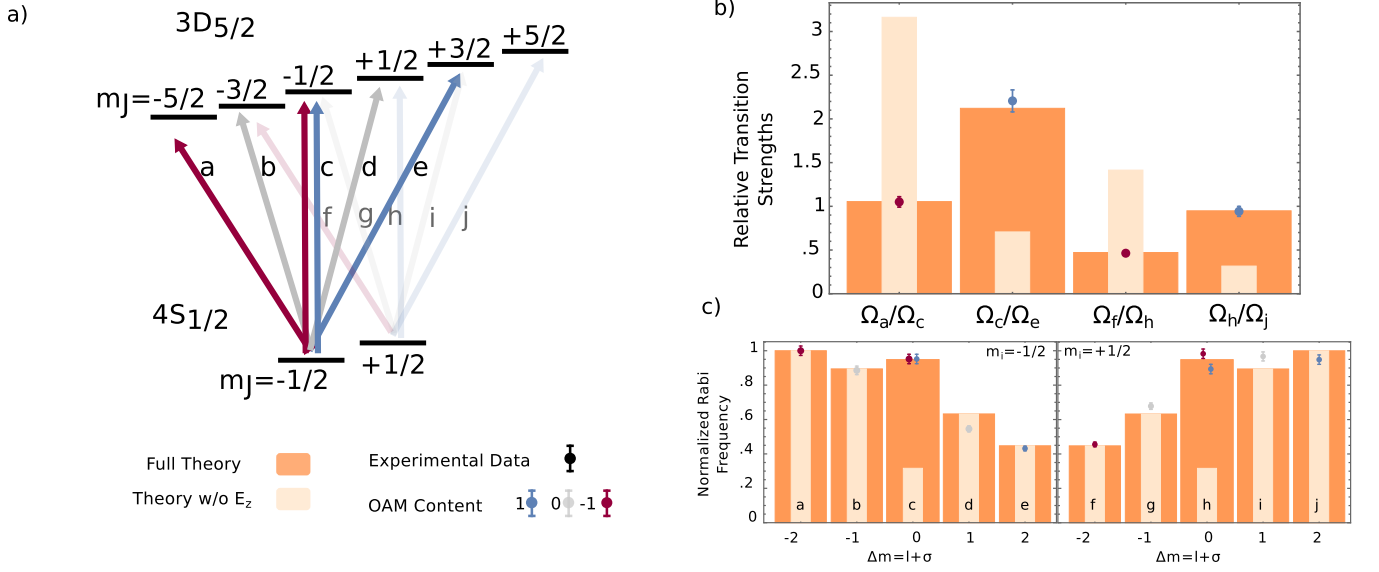


FIG. 1. a) Energy levels for the Zeeman split $^{40}\text{Ca}^+$ quadrupole $S_{1/2}$ - $D_{5/2}$ transition. The transitions are labeled from a to j and shown in different colors indicating the photon orbital angular momentum content. Note that there are two different configurations to drive the $\Delta m = 0$ transitions, either with $\ell = +1$ or -1 . b) Relative transition strengths expressed as ratios of Rabi frequencies Ω for different transition. Data for the $\ell = 1$ transitions (light-blue) and for the $\ell = -1$ (dark-purple) are plotted together with theory predictions. Dark orange bars show the prediction with the model presented in this paper where longitudinal fields are taken into account. Light orange bars show the prediction where the longitudinal field is neglected. c) Normalization is done to a chosen transition Ω_a and to account for the difference in interaction strength between transitions driven with Gaussian or vortex beams with $\Omega_{\text{norm}} = \Omega_a(\delta_{|\ell|,1} + \delta_{\ell,0}kw_0)$. All measured transition strengths and predictions are labeled as in a).

We contrast our theory with recently measured interaction strengths of different quadrupole transitions of a single trapped Calcium ion induced by LG beams, as reported in Ref. [32]. In particular we concentrate on the experiments where the trapped ion is illuminated by on-center [35] LG beams with different polarizations. The LG beam is tuned to the different magnetic sublevels of the $4S_{1/2} - 3D_{5/2}$ transition which are Zeeman-split by a static magnetic field in the z direction (see Fig. 1a). Transitions with different change in atom angular momentum $\Delta m = -2, -1, 0, 1, 2$ were excited with all combinations of spin and orbital angular momentum of the beam $m_p = \sigma + \ell$. Here, we restrict to the cases where the total angular momentum of the photon matches the change of angular momentum of the atom $\Delta m = m_p$. The experiments determined the strength of each transition by measuring the frequency of its Rabi oscillations by state-dependent fluorescence [36]. The Rabi frequencies are proportional to the matrix element of the transition.

To complete the evaluation of matrix elements and comparison with experimental data we follow this algebraic manipulations [37]: we *i*) rewrite the interactions in terms of products of spherical tensors using $\sin(\theta)\exp(\pm i\varphi) = \mp\sqrt{8\pi/3}T_{\pm 1}^{(1)}$ and $\cos(\theta) = \sqrt{4\pi/3}T_0^{(1)}$; *ii*) convert products of lower-rank tensors $\{T_{q_1}^{(k_1)}, T_{q_2}^{(k_2)}\}$ into sums of single higher-rank tensors

$T_q^{(k)}$ times Clebsch-Gordan coefficients with $T_{q_1}^{(k_1)}T_{q_2}^{(k_2)} = \sum_{kq} T_q^{(k)}(kq|k_1k_2q_1q_2)$; *iii*) regroup interaction terms by orbital and spin angular momentum $H_I(\ell, \sigma)$; *iv*) use the Wigner-Eckart theorem to calculate matrix elements $\langle 3D_{5/2}, m_j | H_I(\ell, \sigma) | 4S_{1/2}, m_j \rangle$ (with and without H_{Iz}) and their ratios.

To exemplify the previous procedure we outline the particular case of transitions c and e . These are driven by a field with $\ell = 1$, with $\sigma = -1$ and $\sigma = 1$, with corresponding matrix elements $M_c = \langle 3D_{5/2}, -1/2 | H_I(1, -1) | 4S_{1/2}, -1/2 \rangle$ and $M_e = \langle 3D_{5/2}, 3/2 | H_I(1, 1) | 4S_{1/2}, -1/2 \rangle$. Steps *i*-*iii*) above lead to

$$H_I(1, 1) = -\frac{4\pi}{3}\alpha\rho^2 T_{+2}^{(2)} \quad (5a)$$

$$H_I(1, -1) = \frac{4\pi}{3}\alpha\rho^2 \left[\frac{nT_0^{(2)}}{\sqrt{6}} - \frac{T_0^{(1)}}{\sqrt{2}} \right], \quad (5b)$$

where we introduced the integer n to encompass both cases in one formula: $n = 3$ for the full Hamiltonian $H_I^{(+)} = H_{I\perp}^{(+)} + H_{Iz}^{(+)}$ and $n = 1$ for the case where we omit the longitudinal field $H_I^{(+)} = H_{I\perp}^{(+)}$. The Wigner-Eckart theorem requires the calculation of Clebsch-Gordan coefficients, coupling tensor indices (k, q) , initial-state indices (J, m_j) and final-state indices $(J', m_{j'})$. In our case, these

Clebsch-Gordan coefficients are nonzero only for tensors of rank $k = 2$. Moreover, given that all matrix elements share the same initial and final radial and total angular momentum quantum numbers, the reduced matrix element is the same for all M_γ . Then, the ratio of matrix elements depend on both, the specific prefactors arising from the decomposition of tensor products and the Clebsch-Gordan coefficients arising from the Wigner-Eckart theorem. The predictions for the ratios without and with E_z are

$$\text{case } E_z = 0 : \quad \left| \frac{M_c}{M_e} \right| = \frac{1}{\sqrt{2}} \simeq 0.707 \quad (6)$$

$$\text{case } E_z \neq 0 : \quad \left| \frac{M_c}{M_e} \right| = \frac{3}{\sqrt{2}} \simeq 2.123. \quad (7)$$

These are to be compared to the ratio of power-normalized Rabi frequencies $\Omega_\gamma \propto M_\gamma$. The experimental value for the ratio $\Omega_c/\Omega_e = 2.21 \pm 0.13$, see Fig. 1b. This matches the theory that includes the excitation by the longitudinal field component, but is off from the theory with $E_z = 0$ by more than 11 standard deviations.

In this spirit, we calculate all other matrix elements and compare them to the experimental data for transitions induced by opposite polarizations with the same LG beam, either with $\ell = 1$ (light-blue) or $\ell = -1$ (dark-purple), and for the two possible initial states, see Fig. 1b. Together with the data, we plot the predictions with and without the longitudinal field. We see that the results match the theory with the full vector field. The incomplete theory is off in all cases by more than 11 standard deviations.

The interaction of matter with strong inhomogeneous fields shows complex features and exposes new physics. Our results on the interaction of Laguerre-Gaussian modes with single ions demonstrate that an extremely good quantitative match between predictions and measurements is achieved only if an improved version of the paraxial approximation is used, where the longitudinal field is taken into account. In contrast, a theory that lacks the longitudinal component misses the experimental values for up to 11 standard deviations.

The relative contributions to the interaction strength of the longitudinal and transverse components in a beam with $\ell = 1$ does not depend on the beam waist w_0 , it is only determined by the relative sense of spin and orbital angular momenta.

Longitudinal fields are important in quantum optics setups, such as trapped ions, but also well beyond as for instance for neutral atoms, molecules and quantum dots. Our finding of the significance of longitudinal fields may pave new ways to manipulate matter for spintronics, nanophotonics and quantum information. But besides possible new uses, countless applications thought to be implemented by more technically-demanding tools of near-field optics or tight focusing may become addressable by simple beams of twisted light. One impor-

tant example is the chiral light-matter interaction from the longitudinal component of light propagating in sub-wavelength waveguides to produce directional coupling in nano-photonics chips [28]. In the future, we plan exploring chiral coupling effects from free-propagating LG light beams, specifically for the different platforms of trapped ions or colloidal quantum dots.

* gquinteiro@df.uba.ar

- [1] L. Novotny and B. Hecht, *Principles of nano-optics* (Cambridge university press, 2012).
- [2] Q. Zhan, *Vectorial optical fields: Fundamentals and applications* (World Scientific, 2013).
- [3] R. Dorn, S. Quabis, and G. Leuchs, Phys. Rev. Lett. **91**, 233901 (2003).
- [4] H. Wang, L. Shi, B. Lukyanchuk, C. Sheppard, and C. T. Chong, Nature Photonics **2**, 501 (2008).
- [5] M. Meier, V. Romano, and T. Feuer, Applied Physics A: Materials Science & Processing **86**, 329 (2007).
- [6] Y. Saito, M. Kobayashi, D. Hiraga, K. Fujita, S. Kawano, N. Smith, Y. Inouye, and S. Kawata, Journal of Raman Spectroscopy **39**, 1643 (2008).
- [7] Q. Zhan, Optics express **12**, 3377 (2004).
- [8] X. Zambrana-Puyalto, X. Vidal, and G. Molina-Terriza, Nature communications **5** (2014).
- [9] L. Allen, M. W. Beijersbergen, R. J. C. Spreeuw, and J. P. Woerdman, Phys. Rev. A **45**, 8185 (1992).
- [10] M. Padgett, J. Courtial, and L. Allen, Physics Today **57**, 35 (2004).
- [11] D. L. Andrews and M. Babiker, *The angular momentum of light* (Cambridge University Press, 2012).
- [12] M. J. Padgett, Optics Express **25**, 11265 (2017).
- [13] S. Franke-Arnold and N. Radwell, Optics and Photonics News **28**, 28 (2017).
- [14] G. F. Quinteiro and T. Kuhn, Phys. Rev. B **90**, 115401 (2014).
- [15] G. Quinteiro, D. Reiter, and T. Kuhn, Physical Review A **91**, 033808 (2015).
- [16] N. Bokor, Y. Iketaki, T. Watanabe, and M. Fujii, Optics Express **13**, 10440 (2005).
- [17] Y. Iketaki, T. Watanabe, N. Bokor, and M. Fujii, Opt. Lett. **32**, 2357 (2007).
- [18] P. B. Monteiro, P. A. M. Neto, and H. M. Nussenzveig, Phys. Rev. A **79**, 033830 (2009).
- [19] V. V. Klimov, D. Bloch, M. Ducloy, and J. R. Leite, Phys. Rev. A **85**, 053834 (2012).
- [20] J. R. Zurita-Sánchez and L. Novotny, JOSA B **19**, 2722 (2002).
- [21] E. Pazy, E. Biolatti, T. Calarco, I. D'amico, P. Zanardi, F. Rossi, and P. Zoller, EPL (Europhysics Letters) **62**, 175 (2003).
- [22] B. Sbierski, G. Quinteiro, and P. Tamborenea, Journal of Physics: Condensed Matter **25**, 385301 (2013).
- [23] L. West and S. Eglash, Applied Physics Letters **46**, 1156 (1985).
- [24] A. E. Siegman, *Lasers* (University Science Books, Mill Valley, CA, 1986) p. 276.
- [25] M. Lax, W. H. Louisell, and W. B. McKnight, Physical Review A **11**, 1365 (1975).

- [26] C. G. Chen, P. T. Konkola, J. Ferrera, R. K. Heilmann, and M. L. Schattenburg, *JOSA A* **19**, 404 (2002).
- [27] S. M. Barnett and L. Allen, *Optics communications* **110**, 670 (1994).
- [28] P. Lodahl, S. Mahmoodian, S. Stobbe, A. Rauschenbeutel, P. Schneeweiss, J. Volz, H. Pichler, and P. Zoller, *Nature* **541**, 473 (2017).
- [29] B. Vermersch, P.-O. Guimond, H. Pichler, and P. Zoller, *Physical Review Letters* **118**, 133601 (2017).
- [30] D. L. Andrews, *Structured light and its applications: An introduction to phase-structured beams and nanoscale optical forces* (Academic Press, 2008).
- [31] R. Loudon, *Physical Review A* **68**, 013806 (2003).
- [32] C. T. Schmiegelow, J. Schulz, H. Kaufmann, T. Ruster, U. G. Poschinger, and F. Schmidt-Kaler, *Nature communications* **7**, 12998 (2016).
- [33] G. Quinteiro, D. Reiter, and T. Kuhn, *Physical Review A* **95**, 012106 (2017).
- [34] M. O. Scully and M. S. Zubairy, *Quantum Optics* (Cambridge University Press, Cambridge, 1997).
- [35] G. F. Quinteiro, A. O. Lucero, and P. I. Tamborenea, *J. Phys. Cond. Matter* **22**, 505802 (2010).
- [36] T. Sauter, W. Neuhauser, R. Blatt, and P. E. Toschek, *Phys. Rev. Lett.* **57**, 1696 (1986).
- [37] C. Schmiegelow and F. Schmidt-Kaler, *European Physical Journal D* **66**, 1 (2012).